A Simple Solution-Based Method to Prepare Honeycomb-Like Li$_2$S/Graphene Composite for Lithium-Sulfur Batteries

Jia shunxin, Chen xiuping, Ping Fan[*]*, Zhengping Zhao, Feng Chen, Mingqiang Zhong*

College of Materials Science and Engineering, Zhejiang University of Technology, Hangzhou 310014, China
[*]E-mail: fanping@zjut.edu.cn

In solution-based method, the nature of the solvent may play an important role to the nanostructure of Li$_2$S/graphene composite. In this paper, considering anhydrous N-methylpyrrolidone (NMP) has good wetting ability with graphene and its function groups has high binding energies with Li$_2$S, NMP was used as solvent to prepare Li$_2$S/graphene composite. The structure morphology and electrochemical performance of as-prepared Li$_2$S/graphene composite were investigated. Results show that numerous of nano-Li$_2$S affiliate on graphene surface homogeneously. The existence of these nano-Li$_2$S alleviate π-π interaction between graphene sheets, and Li$_2$S/graphene composite exhibits honeycomb-like structure with abundant micropores. Due to this special structure, without extra treatment, the as-prepared Li$_2$S/graphene composite exhibits improved electrochemical performance, such as high columbic efficiency, high energy capacity, a high rate capability, and a low potential barrier.

Keywords: Lithiume-sulfur battery, Cathode, Lithium sulfide, Graphene

1. INTRODUCTION

High energy rechargeable batteries are in increasingly high demand owing to the increasing use of electric vehicles and portable electronics. lithium−sulfur (Li−S) batteries are regarded as promising candidates for next-generation rechargeable batteries owing to their high theoretical capacity and environmental friendliness.[1-4] However, for a traditional Li−S battery systems, the sulfur cathode is still challenged by a few issues. First, the insulativity of sulfur reduces the utilization of active materials in cathode. Second, the large volume change (80%) occurs in the sulfur electrode during discharge/charge process, resulting in mechanical degradation. Third, the "shuttle effect" of polysulfides causes a huge loss of active materials, and self-discharge. Last but most important issue is

that it is required to employ metallic lithium as an anode, which typically gives rise to dendrite formation and safety problems.

In this regard, lithium sulfide (Li_2S), the fully lithiated state of sulfur with a theoretical capacity of 1166 mAh g^{-1}, is a more desirable cathode material compared to sulfur as it can be paired with some other promising lithium metal-free anodes, such as graphite, tin and silicon [5-16]. Morever, since Li is incorporated into the structure of Li_2S, the electrode shrinks in delithiation and provides sufficient space to endure volume expansion of sulfur in lithiation, leading to enhanced cycle performances for Li−S batteries. [17-21]. However, similar to sulfur, bulk Li_2S particles still suffers from low electronic conductivity, low lithium-ion diffusivity, high charge transfer resistance and serious shuttle effect[14, 22, 23] of lithium polysulfides into the liquid electrolyte, resulting in a large initial activation energy barrier (huge over-potential)[23-29], low columbic efficiency and rapid capacity degradation.

Many strategies have been proposed to circumvent the above issues. According to their different purposes, these methods can be divided into two categories: (i) Reducing the energy barrier by using electrolyte additives or decreasing the particle size of Li_2S. and (ii) boosting electrical transport by accelerating the electrical transport via structure engineering of insulating Li_2S, which usually is done by forming a composite with conducting materials. Earlier attempts focused on fabricating Li_2S-metal composites, while more recent studies have focused on the formation of Li_2S-carbon composites.

Since graphene has high electrical conductivity, good flexibility and large specific surface area ，It exhibits enormous potentials as Li_2S host. Up to now, there has been some works focused on the scalable synthesis for graphene/Li_2S cathode for high-performance lithium sulfur batteries. For sample, Tu et. al. [30] constructed a Li_2S-based composite cathode with the help of three dimensional reduced graphene oxide(3D-rGO) network and outer carbon coating. He et. al.[31] synthesized a three-dimensional Li_2S/graphene hierarchical architecture by depositing highly-crystalline Li_2S nanoparticles into three-dimensional graphene foam network grown by chemical vapor deposition (CVD). Wang et. al.[32] developed a three-dimensional porous composite where Li_2S/C nanoparticles are intimately anchored on the surface of 3D-rGO. Although these synthesized Li_2S/graphene cathode exhibit high discharge capacity, their preparation process is relatively complicated[33] which restricts their application in industrial large-scale production.

Facile preparation of Li_2S/graphene cathode could be provide by solution-based method[34-37]. In this method, commercial Li_2S was dissolved in an organic solvent first, and then mixed with graphene sheets to prepare Li_2S/graphene cathode. Thus, in solution-based method, the nature of the solvent, especially its wetting ability to graphene and its binding energies with Li_2S, may play an important role to the affinity of Li_2S and graphene. At present, almost all solution-based methods reported used anhydrous ethanol as solvent to prepare Li_2S/graphene. Due to the poor wetting between anhydrous ethanol and graphene, in this case, graphene sheets have high tendency of agglomeration owing to van der Waals interactions，which decreases the accessible active sites located on the surface of graphene. Therefore, Li_2S particles were loosely anchored on the surface of graphene, resulting in limited effect on suppression of "shuttle effect" and the resulting low discharge capacity [38]. In order to improve the electrical transport of obtained cathodes, Wu et al. had to mix these

graphene/Li$_2$S sheets with conductive carbon[37] and Yushin[39] et. al. had to further enclosed these graphene/Li$_2$S sheets in protective carbon shells by vapor deposition approaches.

As mentioned above, in solution method, composite structure might be affected greatly by the nature of the solvent. Thus we think if we can find a solvent which not only have binding energies with commercial Li$_2$S powder but also have good wetting ability with graphene surface, nano-size Li$_2$S might closely deposit on conductive graphene sheet during solvent evaporation process. And thus a high performance Li$_2$S/graphene cathode might be obtained without additional treatment or additions. From literature, it has been revealed that the binding energies of the pyrrole ring within PVP with Li$_2$S are higher than those of other functional groups such as amides, ketones, fluoroalkanes, and so on[40]. Thus, we think of anhydrous N-methylpyrrolidone (NMP), which also has pyrrole ring as PVP and has good wetting ability with graphene[41], might be an ideal solvent. In this paper, Li$_2$S/graphene composite was prepared by NMP-based solution method. The structure, morphology and electrochemical performance of obtain composite were investigated.

2. EXPERIMENTAL SECTION

2.1. Materials

Lithium trifluoromethanesulfonate (LiCF$_3$SO$_3$, 98%, Alfa Aesar), lithium nitrate (LiNO$_3$, 99%, Alfa Aesar), dimethoxy ethane (DME, 99%, Alfa Aesar), 1,3-dioxolane (DOL, 99.5%, Alfa Aesar), lithium sulfide (Li$_2$S, 99.98%, Alfa Aesar), and anhydrous N-methyl-2-pyrrolidinone (NMP, Aladdin), Amorphous carbon (Super-P, MMM) were purchased and used as received.

2.2. Preparation of Li$_2$S/graphene composite

Since Li$_2$S is moisture-sensitive, all the preparation were manufactured in the glove box (O$_2$ and H$_2$O concentration <0.1 ppm). Graphene, synthesized according to our previous work[42-44], were first dried at 120°C under vacuum overnight before being transferred to the glove box (O$_2$ and H$_2$O concentration <0.1 ppm) . 0.3g Li$_2$S powder was dissolved in anhydrous 1-methyl-2 pyrrolidone (NMP, Aladdin), and stirred overnight at room temperature. Then, 0.15 g of graphene powders were uniformly dispersed into the above Li$_2$S/NMP solution by continuously stirring for 3 h at the room temperature. Finally, the Li$_2$S/graphene composite were formed by evaporating NMP at 130°C for 5 h under stirring. For comparison, the Li$_2$S/Super-P composite was obtained as the same way without PVP.

2.3. Materials characterizations

X-ray diffraction (XRD) patterns were recorded on X'Pert PRO instrument with Cu Ka radiation from 10° to 80° with the scanning rate was 1° min^{-1}, and the samples were sealed by the Kapton tape. The morphological characterizations were conducted with a JEOL JSM-7800F field

emission scanning electron microscopy (SEM). The elemental mapping was performed with energy-dispersive X-ray spectroscopy (EDX) attached to the SEM.

2.4. Electrochemical Characterization.

Because lithium sulfide is very sensitive to moisture, the electrode preparation and the assembly of coin-type cells were conducted in an argon-filled glovebox in which the moisture level was below 1 ppm. The active material (Li_2S/graphene or Li_2S/Super-P) was mixed and PVDF in a weight ratio of 90:10, and then the mixtures were dispersed in N-methyl-2-pyrrolidinone (NMP) to form slurry. The obtained slurry was uniformly casted onto an aluminum foil and then dried at 120°C for 5 h under Ar atmosphere. The mass loading of the working cathode is around 1.0 mg cm^{-2}.

CR2025 coin-type cells were employed to evaluate the electrochemical properties of the working cathodes. The coin cell was assembled by using Cellgard membrane as a separator and lithium-metal foil as the counter electrode, in which 1 M lithium bis(trifluoromethanesulfonyl)imide (LiTFSI) solution of 1,3-dioxolane (DOL) and 1,2-dimethoxyethane (DME) (1:1 v/v) containing 1 wt.% $LiNO_3$ was used as the electrolyte. The cells were equilibrated for 24 h before operation.

The galvanostatic charge and discharge tests of the coin cells were conducted using a Neware battery testing system at 30°C. Cyclic voltammetry data were collected by using CHI650B electrochemical workstation (Chenhua, Shanghai) at a scan rate of 0.1 m V s^{-1}. The voltage was charged from open circuit voltage to 4.0 V in the initial cycle and the voltage window was switched to 1.5 to 3.0 V in the following discharge/charge cycles. Electrochemical impedance spectroscopy (EIS) measurements were performed with a CHI650B electrochemical workstation in the frequency range of 1 MHz to 0.01 Hz.

3. RESULT AND DISCUSSION

3.1. Microstructure and morphology

X-ray diffraction (XRD) was performed to investigate the crystal structure of the Li_2S/graphene composite, and the XRD pattern was shown in Figure 1. The XRD diffractions of Li_2S and graphene were also presented for comparison. As shown in Figure 1, the XRD patterns of the graphene showed an broad peak centered at 23°, which could be indexed as the (002) reflection and corresponded to stacking of graphene layers[45, 46]. The characteristic XRD peaks of Li_2S at 27.0, 31.2, 44.8, 53.1, 55.6, 65.2, 71.9 and 74.1°, which correspond to the (111), (200), (220), (311), (222), (400), (331) and (420) planes of Li_2S phase (JCPSD 65-2981), were detected in both commercial Li_2S and Li_2S/graphene composites. But in XRD pattern of Li_2S/graphene composites, these peaks were broader, indicating the nucleated Li_2S crystals might be smaller. According to the Scherrer equation[47, 48], the calculated size of Li_2S nanocrystals was about 7.1 nm. Moreover, compared with XRD pattern of the graphene, the (002) diffraction peak of graphene at about 23° in XRD pattern of

Li$_2$S/graphene became so weak that it is almost overlapped with the (111) peak of Li$_2$S, suggesting that Li$_2$S was successfully embedded onto graphene sheets[23].
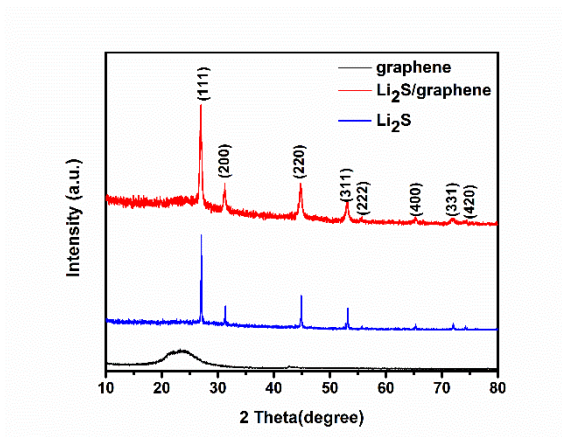

Figure 1. XRD patterns of graphene, Li$_2$S and Li$_2$S/graphene composites
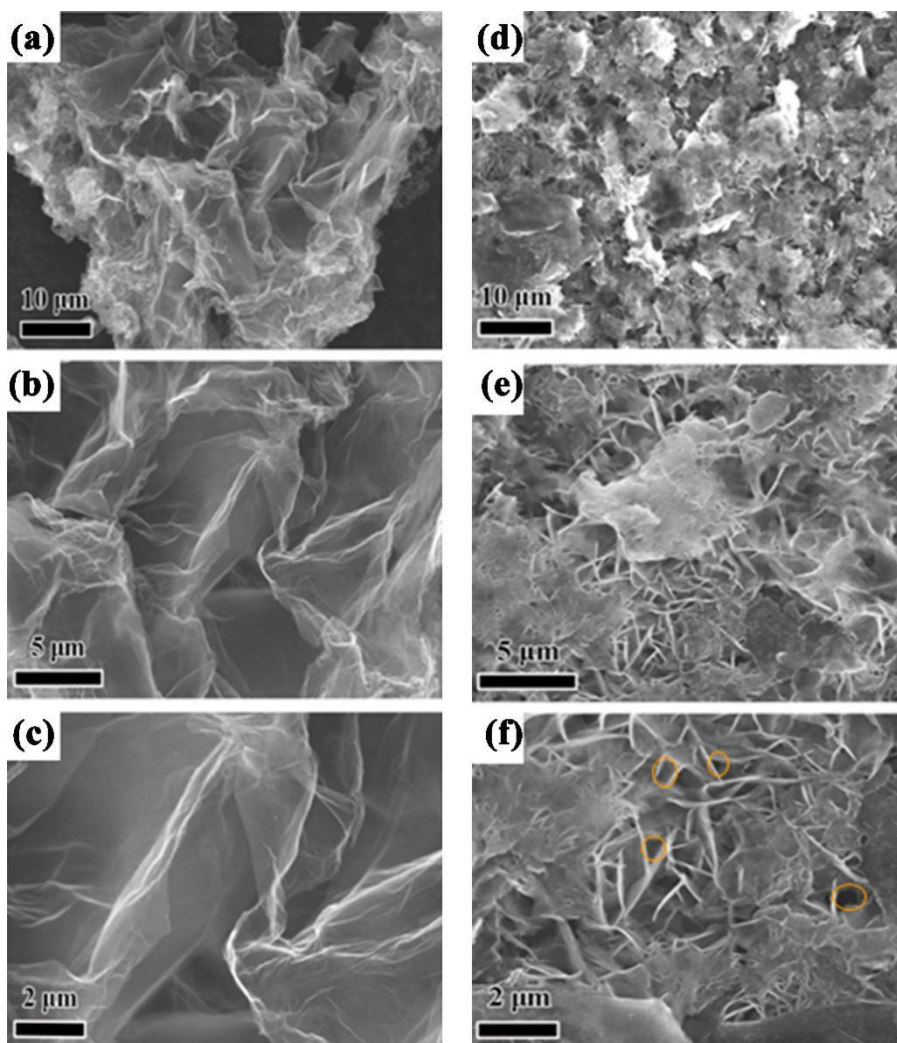

Figure 2. SEM micrograph of graphene (a, b, c) and Li$_2$S/graphene composites (d, e, f) with different magnification
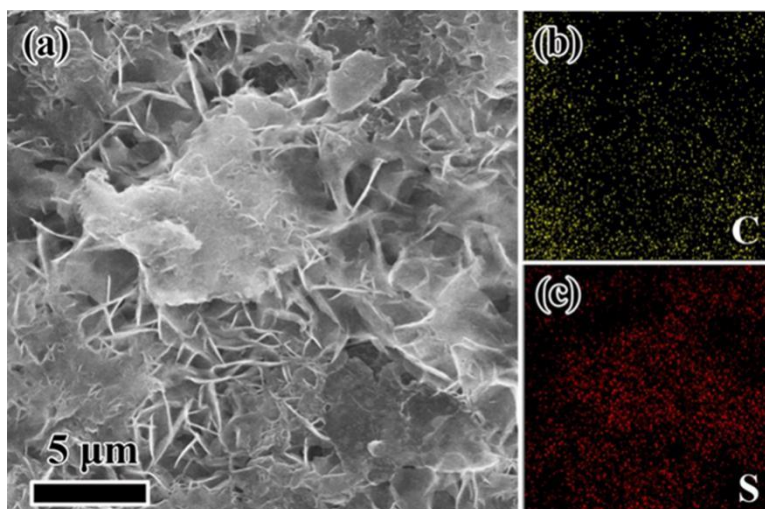
Figure 3. A SEM image of (a) Li_2S@graphene composite and the corresponding EDS mapping for the element distribution (b) C, (c) S.

Scanning electron microscopy (SEM) characterization was conducted to investigate the microstructure of Li_2S/graphene composites, as shown in Figure 2. For comparison, SEM image of graphene were also shown as Fig. 2a-c as well. It could be clearly seen that a typical morphology of the graphene exhibited thin sheet-like structure with slightly curved edges and overlaps each other. The wrinkled surface textures of graphene contributed to the formation of the large specific surface area which combined the remaining functional groups on its surface may offer nucleation and anchoring sites for the Li_2S nanocrystals. After Li_2S deposition, the clean surface of graphene sheets turned to be rugged due to introduction of Li_2S nanospheres. More winkles could be observed on the surface of Li_2S/graphene composite and it exhibited a honeycomb-like structure with abundant internal voids (the size of voids is around 200−500 nm, as indicated by orange circles). It could also be seen that compared with the thickness of graphene sheets (Fig. 2c), the Li_2S/graphene sheets were slightly thicker (Fig. 2f), resulting from the Li_2S deposition. Interestingly, as shown by images in Fig. 2d-f, the Li_2S nanoparticles could not be detected on the surface of Li_2S/graphene sheets even at the high-magnification SEM image (Fig. 2f). It suggested that the size of Li_2S nanoparticles is very small or the Li_2S nanoparticles have been encapsulated in graphene sheets. To clearly demonstrate the elemental distributions of Li_2S/graphene composite, EDS mapping was used, as shown in Fig. 3. The EDS elemental maps of carbon (Figure 3b) and sulfur (Figure 3c) did not show agglomerated sulfur clusters, demonstrating that Li_2S were homogeneously distributed in the Li_2S/graphene composite.

Figure 4 presented a scheme to illustrate why this honeycomb-like structure could be formed in Li_2S/graphene composite through NMP solution method. Since NMP contains an pyrrole ring, when it mixes with commercial Li_2S，the carbonyl groups on pyrrole ring hold tightly with Li_2S[40] and form a Li_2S/NMP solution. On the other hand, the pyrrole ring on NMP molecular exhibits a conjugated π-ring structure. When graphene sheets are added into Li_2S/NMP solution, NMP molecules can also bind strongly to graphene sheets by π–π interactions and alleviate the their aggregation tendency. Therefore, NMP not only can act as a good dispersion solvent for graphene but also can play an role as a introducer of Li_2S to graphene surface. When NMP evaporating, two processes occur simultaneously:

1. Li$_2$S nano crystal deposit on graphene surface and prevent the graphene sheets from agglomeration. 2. the large graphene sheets began to wrinkle to reduce its surface energy. These two simultaneous processes lead the morphology observed in Figure 3a, where Li$_2$S nanoparticles are wrapped by a thin graphene sheet. With NMP evaporation process continues on, the Li$_2$S deposition and wrapping proceed simultaneously and finally result a Li$_2$S/graphene composite with honeycomb-like structure.
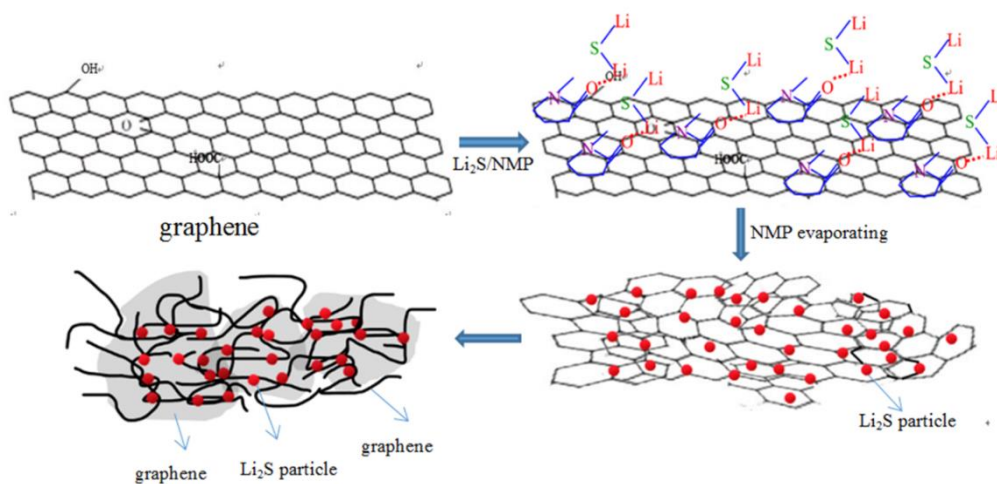

Figure 4. Schematic of the process for the formation of honeycomb-like Li$_2$S/graphene composite based on NMP based solution method

3.2 Electrochemical property

The electrochemical properties of Li$_2$S/graphene composites were investigated in order to evaluate its electrochemical properties. Fig. 5b showed the cyclic voltammetry (CV) curves of Li$_2$S/graphene composite. For comparison, the CV performance of Li$_2$S/Super-P was also measured and the result was shown in Fig. 5a. In order to electrochemically activated the Li$_2$S electrodes, a high activation voltage (4.0 V) was applied in order to overcome the kinetic barrier caused by phase nucleation of polysulfide intermediates. An anodic peak at 3.88 V was observed in the initial scanning of Li$_2$S/Super-P electrodes, whereas two anodic peak could be detected in the Li$_2$S/graphene electrodes and moved to lower voltage, the anodic peak of Li$_2$S/graphene composite at 3.73V and the shoulder peak at 3.33 V in the initial scanning. The movement of anodic peaks indicates that the Li$_2$S/graphene and Li$_2$S/Super-P electrodes possess different electrochemical activation barriers. The electrochemical activation kinetics of Li$_2$S/graphene composite is improved compared to that of Li$_2$S/Super-P. In the following cycles, both Li$_2$S/Super-P and Li$_2$S/graphene composites exhibited one anodic peak at 2.4 V and two cathodic peaks at 2.1 and 2.3 V. The anodic peak corresponds to the oxidation of Li$_2$S and Li$_2$S$_2$ to sulfur or Li$_2$S$_8$ while cathodic peaks correspond to the transition from S and/or long-chain polysulfides to low-order polysulfides and then to Li$_2$S$_2$ and/or Li$_2$S [49-52].
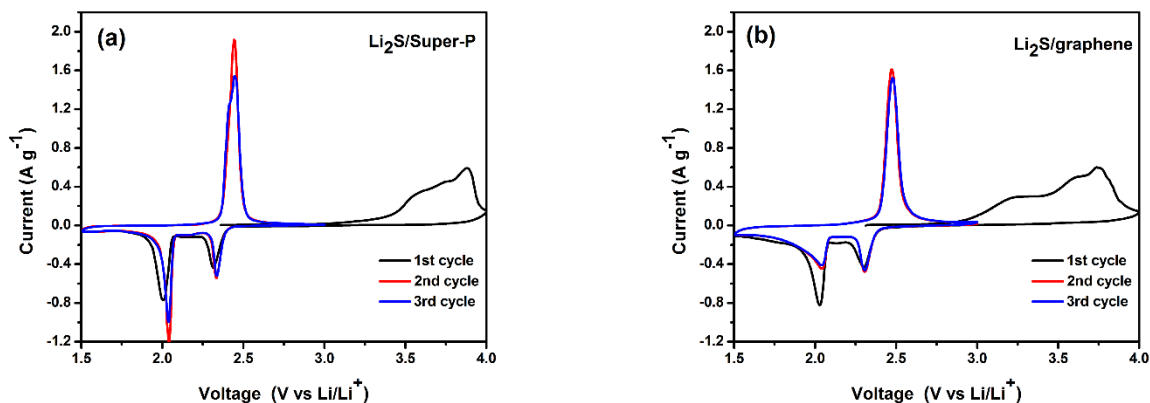
Figure 5. Cyclic voltammograms of (a) Li_2S/Super-P and (b) Li_2S/graphene cathode. All cathodes were charged between 1.5 and 4.0 V for the first cycle and the following three cycles between 1.5 and 3.0 V at a scan rate of 0.1 mV s^{-1}

To investigate the cycling stability of the Li_2S/graphene and Li_2S/Super-P electrodes, the long cycle performance has been studied at the current density of 0.1 A g^{-1} for 100 cycles, as shown in Fig.6. The as-prepared Li_2S/graphene composites exhibited slow capacity fading and high coulombic efficiency. After initial ten cycles, the Li_2S/graphene composites reached a stable discharge capacity of 530 mAh g^{-1}, equal to 760 mAh^{-1} sulfur. The Li_2S/graphene composites still retained 528 and 475 mAh g^{-1}, which equal to 759 and 683 mAh g^{-1} sulfur, of the discharge capacity over 50 and 100 cycles, respectively. For the Li_2S/Super-P composite, the discharge capacity decreased from 483 mAh g^{-1} at 10th cycle to 280 mAh g^{-1} and 156 mAh g^{-1} at 50th and 100th cycle with an average decay rate of 0.76% per cycle, ~7 times greater than that of the Li_2S/graphene composites (0.11%). The Coulombic efficiency of the Li_2S/graphene composites was ~95% in the initial 10 cycles, and gradually increased to ~97% after 50 cycles.

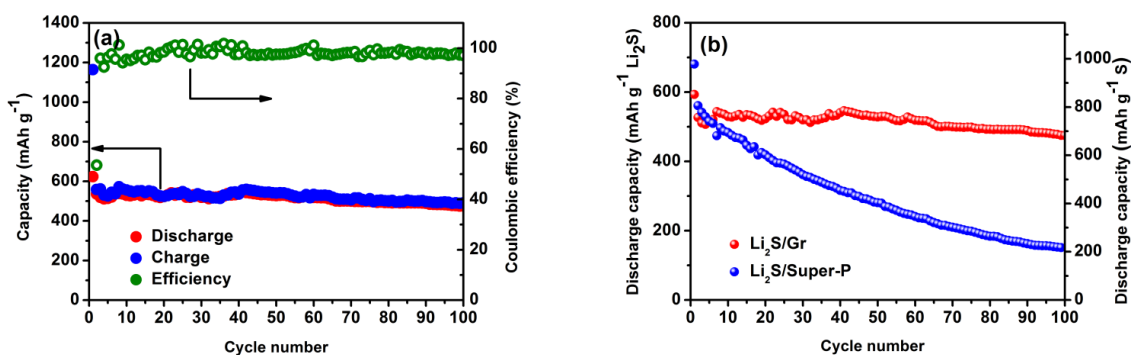**Figure 6.** (a) Cyclability and Coulombic efficiency of Li_2S/graphene nanocomposites at 0.1 Ag^{-1} (b) Comparisons of cycling performance of Li_2S/graphene, Li_2S/Super-P electrodes at 0.1 Ag^{-1}

The rate capability of Li_2S/graphene composites at various current densities from 0.1 A g^{-1} to 1.0 A g^{-1} was investigated to further evaluate the electrode kinetics and cycling stability, as shown in

Fig. 7. The discharge capacities at current density of 0.1, 0.2, 0.5, 1.0 A g^{-1} were around 530, 464, 384 and 325 mAh g^{-1}. It meant that at 0.2, 0.5, 1.0 A g^{-1}, Li$_2$S/graphene cathode showed 87%, 72% and 61% capacity retentions, respectively. In addition, when the current density was switched from 1.0 A g^{-1} back to 0.1 A g^{-1}, the discharge capacity recovered to 512 mAh g^{-1}, which remained 96% of its 10th-cycle capacity. All these results implied that the Li$_2$S/graphene cathode has good reversibility and high-rate capability.
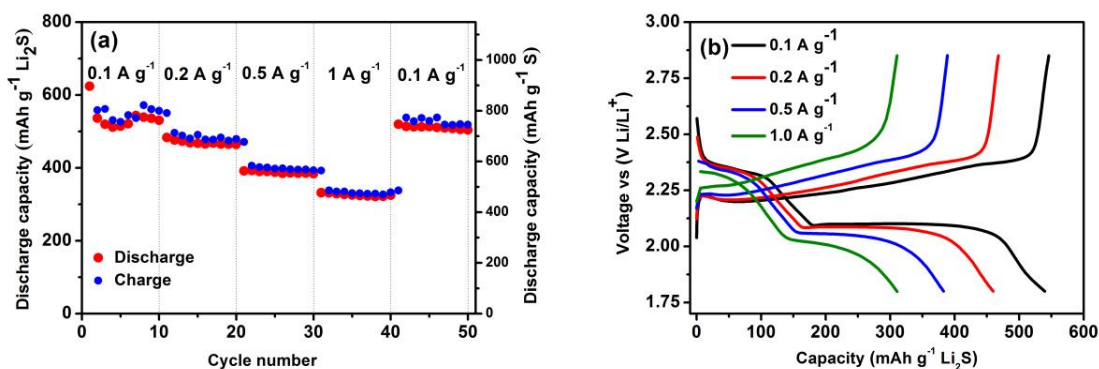

Figure 7. (a) Rate capability of Li$_2$S/graphene composites. (b) Discharge/charge voltage profiles of Li$_2$S/graphene profiles of Li$_2$S/graphene

Table 1. Comparison of electrochemical performance of Li$_2$S/graphene electrodes

Cathode (without extra treatment for improving electron conductivity)	Loading （mg cm^{-2}）	Li$_2$S wt%	Rate A g^{-1}	Initial discharge capacity （mAh g^{-1}）	Stable discharge capacity （mAh g^{-1}） and cycles	Ref
Li$_2$S/graphene prepared by alcohol solution method	2.5-3.5	75%	0.1	510	290	[56]
Li$_2$S/graphene prepared by NMP solution method	~1.0	66%	0.1	600	491	This work

Fig. 7b showed representative voltage profiles of Li$_2$S/graphene composites at different charge/discharge rate. For consideration of stability, we chose the voltage profile at the 5th cycle of each different charge/discharge rate. Two discharge plateaus in the range of 2.4–2.1 V and 2.1–1.7 V were observed, which were related to the stepwise reactions between Li$_2$S and solid S$_8$ molecules[53-55]. It could be seen that the cell polarization (voltage difference between the first charge voltage plateau and the second discharge voltage plateau) slightly increased from 0.14 to 0.33 V as the rate increased from 0.1A g^{-1} to 1A g^{-1}, revealing decreased utilization of sulfur and increased voltage hysteresis as the charge/discharge rate increased. However, at each different charge/discharge rate, Li$_2$S/graphene composites exhibited a stable plateau , even at the high charge/discharge rate of 1A g^{-1},

demonstrating a good electronic conductivity and low energy loss associated with charge/discharge overpotentials owing to the highly conductive graphene substrate and its close contacts with Li_2S.

Table 1 compared the performance of obtained Li_2S/graphene composites prepared by NMP solution method with Li_2S/graphene composites prepared by alcohol solution method reported in the literature[56]. Li_2S/graphene composites prepared in this paper shows outstanding performance in terms of initial charge voltage, specific capacity, rate capability, and cycle life.

Combining the results of SEM and electrochemical analysis, it could be seen that the fast reaction kinetics, low polarization, and greatly enhanced capacity and rate capability of Li_2S/graphene electrode could be ascribed to the architecture of Li_2S/graphene composite. The increased discharge capacities of Li_2S should be ascribe to the uniform dispersion of nano-size Li_2S. The high conductivity of graphene as well as the close contact between the insulating electroactive material (Li_2S) and graphene matrix are responsible for the improvement of the utilization of active material and also contribute to the transport of electrons to the active material during the charge–discharge process. The internal void space ensures the sufficient accommodation to suppress the volume expansion of sulfur during lithiation, and entrap the intermediate polysulfides.
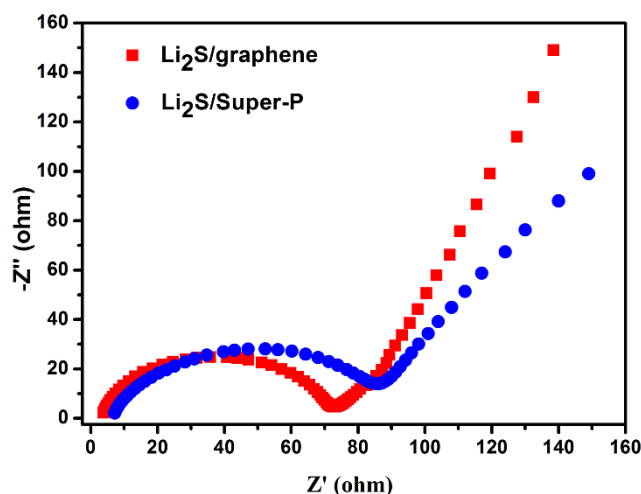

Figure 8. Electrochemical impedance spectroscopy of Li_2S/graphene and Li_2S/Super-P composites

In order to confirm this point, electrochemical impedance spectra measurements were carried out, since it is an effective way to examine the reaction kinetics of cathodes. The Nyquist plots of both samples at the open-circuit voltage were composed of a semi-circle at the high frequency assigned to the charge transfer resistance (R_{ct}) of the electrode and the straight line at the low-frequency region corresponding to a semi-infinite Warburg diffusion process (Z_w). In addition, the junction of the semi-circle at the real axis in high frequency corresponded to the internal resistance (R_s)[57]. The R_{ct} of the Li_2S/graphene composite (74Ω) was lower compared to that of the Li_2S/Super-P composite ($85.4\ \Omega$), which can be attributed to the favorable charge- and ion-transfer processes from the interconnected graphene framework and close contact between Li_2S and graphene. The low value of R_{ct} for Li_2S/graphene composite implies that the shuttle effect of lithium polysulfides and the deposition of

final insulated Li_2S_2/Li_2S have been suppressed by the confinement of graphene layers. Based on the slope of the inclined line in the low frequency range, which is associated with the diffusion impedance[58, 59], it could be known that the lithium ion diffusion coefficient of Li_2S/graphene composites was greater than that of the Li_2S/Super-P. Besides, the lower value of R_s (3.8 Ω) for Li_2S/graphene electrode should be attributed to the improved electrical conductivity by graphene layer and intimate contact of Li_2S particles with conductive graphene matrix

4. CONCLUSION

In summary, we reported a simple method to prepare honeycomb-like Li_2S/graphene composite through NMP solvent-based method. The microstructures, morphology and electrochemical performance of obtained Li_2S/graphene composites were investigated. The Li_2S/graphene exhibits honeycomb-like morphology with abundant micropores where nano-sized Li_2S particles closed contact to or are wrapped by thin graphene sheets. Due to this special structure, without extra treatment, the as-prepared Li_2S/graphene composite shows improved electrochemical performance, such as high columbic efficiency, high energy capacity, a high rate capability, and a low potential barrier. Considering the simple preparation strategy and the special composite morphology, our research may provide a reference for design/preparation of large-scale synthesizable, advanced Li_2S/graphene cathodes.

References

1. J.R. He, Y.F. Chen, P.J. Li, F. Fu, Z.G. Wang, W.L. Zhang, *J. Mater. Chem. A*, 3 (2015) 18605.
2. X.L. Ji, K.T. Lee, L.F. Nazar, *Nat Mater.*, 8 (2009) 500.
3. A. Manthiram, Y.Z. Fu, S.H. Chung, C.X. Zu, Y.S. Su, *Chem. Rev.*, 114 (2014) 11751.
4. M.P. Yu, J.S. Ma, H.Q. Song, A.J. Wang, F.Y. Tian, Y.S. Wang, *Energy Environ. Sci.*, 9 (2016) 1495.
5. M. Agostini, J. Hassoun, J. Liu, M. Jeong, H. Nara, T. Momma, *Acs Appl. Mater. Interfaces,* 6 (2014) 10924.
6. K.P. Cai, M.K. Song, E.J. Cairns, Y.G. Zhang, *Nano Lett.*, 12 (2012) 6474.
7. Y.Z. Fu, C.X. Zu, A. Manthiram, *J. Am. Chem. Soc.*, 135 (2013) 18044.
8. J. Hassoun, B.A. Scrosati, *Angew. Chem.,* 49 (2010) 2371.
9. J. Hassoun, Y.K. Sun, B. Scrosati, *J. Power Sources*, 196 (2011) 343.
10. M. Kohl, J. Bruckner, I. Bauer, H. Althues, S. Kaskel*, J. Mater. Chem. A*, 3 (2015) 16307.
11. X.B. Meng, D.J. Comstock, T.T. Fister, J.W. Elam, *Acs Nano*, 8 (2014) 10963.
12. Z.W. Seh, J.H. Yu, W.Y. Li, P.C. Hsu, H.T. Wang, Y.M. Sun, H.B. Yao, Q.F. Zhang, Y. Cui, *Nat. Commun.*, 5 (2014) 5017.
13. H. Tang, J. Zhang, Y.J. Zhang, Q.Q. Xiong, Y.Y. Tong, Y. Li,X.L. Wang, C.D. Gu, J.P. Tu, *J. Power Sources*, 286 (2015) 431.

14. L. Wang, Y. Wang, Y.Y. Xia, *Energy Environ. Sci.*, 8 (2015) 1551.
15. Y. Yang, M.T. McDowell, A. Jackson, J.J. Cha, S.S. Hong, Y. Cui, *Nano Lett.*, 10 (2010) 1486.
16. Z.C. Yang, J.C. Guo, S.K. Das, Y.C. Yu, Z.H. Zhou, H.D. Abruña, L.A. Archer, *J. Mater. Chem. A*, 1 (2013) 1433.
17. F.Y. Fan, W.C. Carter, Y.M. Chiang, *Adv. Mater.*, 27 (2015) 5203.
18. J.R. He, Y.F. Chen, W.Q. Lv, K.C. Wen, C. Xu, W.L. Zhang, Q. Wu, W.D. He, *Acs Energy Lett.*, 1 (2016) 820.
19. Z.W. Seh, H.T. Wang, N. Liu, G.Y. Zheng, W.Y. Li, H.B. Yao, C. Yi, *Chem. Sci.*, 5 (2014) 1396.
20. D. Sun, Y. Hwa, Y. Shen, Y.H. Huang, E.J. Cairns, *Nano Energy,* 26 (2016) 524.
21. F.X. Wu, J.T. Lee, A. Magasinski, H. Kim, G. Yushin, *Part. Part. Syst. Charact.*, 31 (2014) 639.
22. K. Cai, M.K. Song, E.J. Cairns, Y. Zhang, *Nano Lett.*, 12 (2012) 6474.
23. C. Wang, X.S. Wang, Y. Yang, A. Kushima, J.T. Chen, Y.H. Huang, J. Li, *Nano Lett.*, 15 (2015) 1796.
24. Z. Chenxi, K. Michael, M. Arumugam, *J. Phys. Chem. Lett.*, 5 (2014) 3986.
25. J. Hassoun, B.A. Scrosati, *Angewandte Chemie*, 49 (2010) 2371.
26. S. Meini, E. Ran, A. Rosenman, A. Garsuch, D. Aurbach, *J. Phys. Chem. Lett.*, 5 (2014) 915.
27. Y. Yang, M.T. Mcdowell, A. Jackson, J.J. Cha, S.S. Hong, Y. Cui, *Nano Lett.*, 10 (2010) 1486.
28. Y. Yang, G. Zheng, S. Misra, J. Nelson, M.F. Toney, Y Cui, *J. Am. Chem. Soc.*, 134 (2012) 15387.
29. Y. Son, J.S. Lee, Y. Son, J.H. Jang, J. Cho, *Adv. Energy Mater.*, 5 (2015) 1500110.
30. Y. Chen, X. Ma, X. Cui, Z. Jiang, *J. Power Sources*, 302 (2016) 233.
31. C. Ahn, T. Okada, M. Ishida, E. Yoo, H. Zhou, *J. Power Sources*, 307 (2016) 474.
32. D.H. Wang, X.H. Xia, D. Xie, X.Q. Niu, X. Ge, C.D. Gu, X.L. Wang, J.P. Tu, *J. Power Sources*, 299 (2015) 293.
33. D. Sun, Y. Hwa, Y. Shen, Y. Huang, E.J. Cairns, *Nano Energy*, 26 (2016) 524.
34. Z. Kai, L. Wang, H. Zhe, F. Cheng, J. Chen, *Sci. Rep.*, 4 (2014) 6467.
35. Z.W. Seh, J.H. Yu, W. Li, P.C. Hsu, H. Wang, Y.M. Sun, H.B. Yao, Q.F. Zhang, Y. Cui, *Nat. Commun.*, 5 (2014) 5017.
36. F. Wu, H. Kim, A. Magasinski, J.T. Lee, H.T. Lin, G. Yushin, *Adv. Energy Mater,* 4 (2014) 1220.
37. F. Wu, J.T. Lee, A. Magasinski, H. Kim, G. Yushin, *Part. Part. Syst. Charact.*, 31 (2014) 639.
38. G. Zhou, E. Paek, G.S. Hwang, A. Manthiram, *Adv. Energy Mater*, 6 (2016) 1501355.
39. F. Wu, J.T. Lee, E. Zhao, Z. Bao, G. Yushin, *Acs Nano*, 10 (2016) 1333.
40. W.S. Zhi, Q. Zhang, W. Li, G. Zheng, H. Yao, Y. Cui, *Chem. Sci.*, 4 (2013) 3673.
41. Y. Hernandez, V. Nicolosi, M. Lotya, F.M. Blighe, Z.Y. Sun, S. De, I. McGovern, B. Holland, M. Byrne, Y. Gun'ko, J. Boland, P. Niraj, G. Duesberg, S. Krishinamurti, R. Goodhue, J. Hutchison, V. Scardaci, A.C. Ferrari, J.N. Coleman, *Nat. Nanotechnol.*, 3 (2008) 563.
42. P. Fan, J. Chen, J. Yang, F. Chen, M. Zhong, *J. Nanopart. Res.*,19 (2017) 36.
43. P. Fan, L. Wang, S. Jia, F. Chen, J. Yang, M. Zhong, *J. Appl. Polym. Sci.*, 134 (2017) 44628.
44. P. Fan, L. Wang, J. Yang, F. Chen, M. Zhong, *Nanotechnology.*, 23 (2012) 365702.
45. G. Wang, J. Yang, J. Park, X. Gou, B. Wang, H. Liu, J. Yao*, J. Phys. Chem.* C, 112 (2008) 8192.
46. A.V. Murugan, T. Muraliganth, A. Manthiram, *Chem. Mater.*, 22 (2009) 2692.
47. A.L. Patterson, *Phys. Rev.*,56 (1939) 972.
48. U. Holzwarth, N. Gibson, *Nat. Nanotechnol.*,6 (2011) 534.
49. R. Elazari, G. Salitra, A. Garsuch, A. Panchenko, D. Aurbach*, Adv. Mater.*, 23 (2011) 5641.
50. Y.X. Wang, L. Huang, L.C. Sun, S.Y. Xie, G.L. Xu, S.R. Chen, Y.F. Xu, J.B. Li, S.L. Chou, S.X. Dou, S.G. Sun, *J. Mater. Chem.*, 22 (2012) 4744.
51. N. Jayaprakash, J. Shen, S.S. Moganty, A. Corona, L.A. Archer. *Angew. Chem.*, 123 (2011) 6026.
52. L.W. Ji, M.M. Rao, H.M. Zheng, L. Zhang, Y.C. Li, W.H. Duan, J.H. Guo, E.J. Cairns, Y.G. Zhang, *J. Am. Chem. Soc.*, 133 (2011) 18522.
53. P.G. Bruce, S.A. Freunberger, L.J. Hardwick, J.M. Tarason. *Nat. Mater.*, 11 (2012) 19.
54. X. Ji, L.F. Nazar, *J. Mater. Chem.*, 20 (2010) 9821.

55. J. Shim, K.A. Striebel, E.J. Cairns, *J. Electrochem. Soc.*,149 (2002) A1321.
56. D.H. Wang, D. Xie, T. Yang, Y. Zhong, X.L. Wang, X.H. Xia, C.D. Gu, J.P. Tu, *J. Power Sources*, 313 (2016) 233.
57. J.R. He, Y.F. Chen, W.Q. Lv, K.C. Wen, P.J. Li, F. Qi, Z.G. Wang, W.L. Zhang, Y.R. Li, W. Qin, W.D. He, *J. Power Sources*, 327 (2016) 474.
58. H. Liu, C. Li, H.P. Zhang, L.J. Fu, Y.P. Wu, H.Q. Wu, *J. Power Sources*, 159 (2006) 717.
59. Y. Xia, W. Zhang, H. Huang, Y. Gan, C. Li, X. Tao. *Mater. Sci. Eng.* B., 176 (2011) 633.